WITHDRAWN: Germanium-Doped Coupled Ring-Core Fiber for Extremely Dispersive Orbital Angular Momentum Modes

Wenpu Geng
Nankai University
Yuxi Fang
Nankai University
Yingning Wang
Nankai University
Changjing Bao
University of Southern California
Hao Zhang
Nankai University
Hao Huang
University of Southern California
Yongxiong Ren
University of Southern California
Zhongqi Pan
University of Louisiana at Lafayette
Yang Yue
yueyang@xjtu.edu.cn

Xi'an Jiaotong University

Research Article

Keywords:

Posted Date: February 24th, 2022

DOI: https://doi.org/10.21203/rs.3.rs-1341308/v1

Additional Declarations: No competing interests reported.

EDITORIAL NOTE:

The full text of this preprint has been withdrawn by the authors while they make corrections to the work. Therefore, the authors do not wish this work to be cited as a reference. Questions should be directed to the corresponding author.

Abstract

A coupled ring-core fiber with extremely negative dispersion is proposed, simulated, and analyzed. Featured by two coaxial Ge-doped silica rings, this fiber can support highly dispersive orbital angular momentum (OAM) modes. The dependence of dispersion characteristics on the variable parameters of the fiber is theoretically and systematically investigated, including the geometry parameters and the mole fraction of GeO_2. The order of the supported OAM modes in this fiber can be up to 100, achieving a highly negative dispersion reaching to -44,579 ps/(nm·km) at 1348.4 nm. The operation wavelength and the value of dispersion can be adjusted according to the need by selecting the fiber parameters. Furthermore, by adjusting the GeO_2 concentration, the operation window of the $OAM_{65,1}$ mode can be tuned in a much wider range from 1212.4 nm to 1666.2 nm.

Introduction

With the exponentially increased demand on information transmission capacity, space division multiplexing (SDM) has a promising potential to remove the obstacles in the current optical communication systems [1–5]. Orbital angular momentum (OAM) modes propagating with the unique helical phase profiles have been applied as a multiplexing technique in the spatial domain. The OAM mode with certain topological charge *l* generates by linearly combining even and odd modes of the fiber eigenmodes (EH and HE modes) carrying the same number of intensity rings of the mode *m* as follow:

$$OAM^{\pm}_{\pm l,m} = HE^{even}_{l+1,m} \pm jHE^{odd}_{l+1,m} \quad (1)$$

$$OAM^{m}_{\pm l,m} = EH^{even}_{l-1,m} \pm jEH^{odd}_{l-1,m} \quad (2)$$

where the '±' in superscript of 'OAM' is the direction of the circular polarization, the subscript '±' before *l* denotes the rotation direction of wavefront. OAM modes with varied *l* are mutually orthogonal, contributing to their multiplexing along the same beam axis and demultiplexing with low crosstalk, which introduces a new degree of freedom for SDM systems [6–8]. With the helical phase form, the modal distribution of the OAM mode has a donut shape and a central phase singularity. After decades of profound research, the promising applications of OAM modes have been extended tremendously to classical and quantum communications [9–11], optical trapping [12, 13], and sensing [14, 15].

Ring-core fiber with the annular index distribution has been demonstrated to propagate OAM modes stably, which introduces a feasible medium for OAM propagation [16–18]. S. Ramachandran, *et al.* experimentally demonstrated that ring-core fiber can generate and propagate OAM modes over long distance with unprecedented stability in 2009 [19]. Recent report has shown that > 1000 information-carrying OAM states can be supported in an arsenic trisulfide ring fiber with air fiber core [20], and highly coherent two-octave-spanning OAM spectral broadening could be formed [21, 22]. Silica (SiO_2) has been widely used in manufacturing optical fiber by the industry and research for decades due to its favorable properties and mature preparation methods. Ge-doped silica, which is well compatible with the common

fiber material silica, is also a popular substance in fiber research and drawing [23–27]. In addition, due to the adjustable mole fraction of GeO_2, the material refractive index of it can be tuned flexibly.

Chromatic dispersion (CD) is one of the important design issues for optical fiber in various applications, such as ultrafast optical oscilloscope [28], optical correlation [29], true time-delay beam former [30], and phased array antenna systems [31]. To tailor the dispersion, which is usually positive in the optical fiber communication systems, fiber with large negative dispersion needs to be placed in serial along the optical fiber link. In the recent research and development, fibers with large negative dispersion for the fundamental fiber eigenmode have been reported [32–36].

In this paper, a highly dispersive coupled ring-core fiber (HD-CRF) based on silica and germanium-doped (Ge-doped) silica is proposed. This fiber with two coupled high-index rings can support high order OAM modes characterized by extremely negative dispersion. With properly optimized fiber parameters, the dispersion of $OAM_{100,1}$ mode reaches to -44,579 ps/(nm·km) at the wavelength 1348.4 nm. The feasibility of the proposed fiber shows its potential dispersion-adjusting applications in a variety of OAM transmission systems based on optical fiber.

Results

Structure of the designed OAM HD-CRF

The schematic structure and material refractive index distribution design of the OAM HD-CRF at 1550 nm is depicted in Fig. 1. Here, r_1, r_2, r_3, r_4, Δr_1, Δr_2 and d are variable parameters and the fiber cladding radius r_5 is set as a constant 62.5 μm. This constant is matched to the radius of the common single-mode optical fiber (SMF). The proposed HD-CRF consists of two high-index pure GeO_2 rings in the background of undoped silica. The material refractive indices of the high-index rings and the low-index cladding show a step, which influences the order of the OAM mode supported in this fiber and can be adjusted by changing the concentration of GeO_2 doped in silica.

Property of supported OAM modes

Figure 2(a) depicts the process of negative chromatic dispersion generated in the proposed OAM fiber and Fig. 2(b) shows the simulated mode field intensity and phase distributions of OAM modes with topological charge $|l|$ = 25, 50, 75, 100 supported in this fiber at the most dispersive wavelength by the full vector finite element method (FEM). Here, the modal intensity has an annular distribution, while the phase front is in a helical form. Moreover, when $l_1 > l_2$, the radii of two high-index rings supporting OAM modes with the topological charge l_1 are larger than those supporting OAM modes with l_2. Table 1 summarizes the optimized geometry parameters of HD-CRFs supporting the above OAM modes.

Figure 3(a) illustrates the effective refractive indices n_{eff} with intensity distributions versus wavelength for the $OAM_{100,1}$ mode supported in the inner ring, outer ring and the proposed fiber with two rings by

implementing Sellmeier equations [37, 38]. As wavelength increases, the n_{eff} of the OAM mode in the ring near the fiber core reduces relatively drastically, while the n_{eff} of the same OAM mode in the high-index ring near the cladding decreases more gradual. Therefore, by optimizing the fiber parameters, the n_{eff} curves of $OAM_{100,1}$ mode supported in two rings respectively can intersect at a desired wavelength (λ_0). Consequently, at this wavelength λ_0, there is a great slope variation in the composite index curve of the $OAM_{100,1}$ mode in the designed dual-ring fiber.

Table 1
Fiber geometry parameters and corresponding CD for different order OAM modes.

Mode	$OAM_{25,1}$	$OAM_{50,1}$	$OAM_{75,1}$	$OAM_{100,1}$
r_1 (μm)	11.5	23.5	35	49
r_2 (μm)	13	25	36.5	50.5
r_3 (μm)	16.5	28.5	40	54
r_4 (μm)	17.3	29.5	41.1	55.2
λ_0 (nm)	1469.6	1402.8	1360.2	1348.4
min. dispersion (ps/(nm·km))	-113,619	-90,512	-76,282	-44,579

Figure 3(b) depicts the effective indices n_{eff} of eigenmodes near the $HE_{101,1}$ mode, which compose the $OAM_{100,1}$ mode in this fiber. The n_{eff} difference between eigenmodes ($EH_{98,1}$ mainly supported in the inner ring, $HE_{101,1}$, and $EH_{96,1}$ mainly supported in the outer ring) for HD-CRF with the same structure parameters can be maintained above ~ 10^{-4} over the operating wavelength range to ensure the good separation between eigenmodes.

Figure 4 compares the properties of different order OAM modes supported in the proposed HD-CRF with geometry parameters summarized in Table 1, including the effective mode area A_{eff}, ratio of power integral in the high-index ring near the core to that in ring near the fiber cladding, and chromatic dispersion D. Here, the OAM modes dispersion [39] are calculated from the effective refractive index n_{eff} with wavelength as independent variable as follows:

$$D(\lambda) = \frac{-\lambda}{c}\frac{d^2 n_{eff}}{d\lambda^2} \quad (3)$$

where λ represents the wavelength, c denotes the velocity of the light propagating in the vacuum.

For the sake of clarity, the brief description of the principle for the proposed fiber is explained as follows. As shown in Fig. 3(a) and Fig. 4, when $\lambda < \lambda_0$, the mode supported in this fiber is basically confined in the ring near the fiber core, which leads to the power ratio relatively high. Near the crossing wavelength λ_0, a significant optical coupling occurs. When the mode field distribution moves to ring near the cladding, A_{eff} rapidly increases, and the power ratio decreases to 1. The dispersion of this OAM mode thus has an extremely negative value at the composite refractive index abrupt wavelength λ_0 as shown in Fig. 4(c). As the wavelength further increases, the mode is mainly guided in the ring near the cladding. With the optimized geometrical parameters, the D of the $OAM_{100,1}$ mode reaches downward to -44,579 ps/(nm·km) at 1348.4 nm. Table 1 lists the minimum dispersions and their corresponding wavelength λ_0 of the other OAM modes (l = 25, 50, 75).

Dispersion characteristic

As discussed above, by varying the n_{eff} profiles of the two rings, the value and the position of the minimum dispersion could be changed accordingly. We further investigate the influence of the fiber geometrical and material parameters on chromatic dispersion for the $OAM_{100,1}$ mode.

Figure 5 illustrates the dependence of the chromatic dispersion on the thickness of two concentric germanium-doped rings (Δr_1 and Δr_2). When Δr_1 and Δr_2 increase simultaneously, the most dispersive wavelength is shifted to short wavelength with more negative CD. The minimum dispersion of the $OAM_{100,1}$ mode is reduced dramatically from − 14,145 to -44,579 ps/(nm·km), and λ_0 moves from 1629.2 nm to 1348.4 nm. However, larger width has stronger restrictions on the modes which further limit the mode transition between the inner ring and the outer ring.

Figure 6 displays the dispersion profiles of the $OAM_{100,1}$ mode with different distances between the two Ge-doped rings d from 4.6 to 5 μm while fixing the inner ring and width (r_1 = 49 μm, r_2 = 50.5 μm and Δr_2 = 1.2 μm). When the outer high-index ring is moved away from the fiber core, the position of λ_0 blue-shifts from 1436.2 nm to 1348.4 nm and the most negative dispersion varies from − 9,255 to -44,579 ps/(nm·km). Furthermore, the sacrifice between the full width at half maximum (FWHM) of the dispersive window and the extreme value of CD need to be taken into consideration in the optimization process [40]. When the dispersion is reduced from − 9,255 to -44,579 ps/(nm·km), the FWHM of the dispersive window reduces from 3.4 to 0.6 nm.

Figure 7 depicts the CD profile of the $OAM_{100,1}$ mode in the designed HD-CRF with two doped ring moving towards the cladding in a step of 0.5 μm, while the relative location and thickness of the two regions are constant (d = 5 μm, Δr_1 = 1.5 μm, Δr_2 = 1.2 μm). With the two Ge-doped rings moving 1 μm in the radial direction, λ_0 is increased by 65.6 nm and the extremum of the dispersion rises from − 44,579 to -28,895 ps/(nm·km). Here, the effective refractive index curves for the $OAM_{100,1}$ mode supported independently in the inner and outer rings simultaneously move up, and the decrease in their refractive indices with wavelength is relatively slower. However, the slope of n_{eff} in the inner heavily doped ring increases more.

As the slope difference between the two rings decreases, the most dispersive wavelength shifts and the extreme of CD increases.

Due to the variable mole fraction of GeO_2, the dispersion characteristics of the OAM modes supported in the proposed heavily germanium-doped HD-CRF can be further tailored. To prevent the appearance of radially higher order modes ($m \geq 2$), the thickness of the ring with high index is carefully controlled, which guarantees that only radial fundamental ($m = 1$) OAM modes are supported. As the mole fraction of GeO_2 decreases, the refractive index difference between the ring and the cladding decreases, and thus the OAM modes supported in the low-doped ring fiber are less than that in the high-doped ring fiber under certain ring width. The chromatic dispersion curves of the $OAM_{65,1}$ mode under varying concentration of GeO_2 in the two high-index rings are depicted in Fig. 8. As the mole fraction of GeO_2 increases from 50–100%, the dispersion window is shifted by 453.8 nm to the longer wavelength region and achieves a larger negative dispersion, which is from − 10,773 to -20,152 ps/(nm·km). The structure parameters of the fiber with higher mole fraction can be further optimized to acquire larger negative dispersion. However, there is an increment in the loss as the mole fraction increases, which cannot be neglected in fiber parameters selection.

Conclusions

In summary, we investigated a dual-ring HD-CRF with germanium-doped silica as high-index materials, which could support highly dispersive OAM modes. With the intense coupling between the modes distributed in the two rings, the negative dispersion for the $OAM_{100,1}$ mode reaches to -44,579 ps/(nm·km) at 1348.4 nm. The numerical results indicate that the working wavelength window is mainly dependent on the effective refractive indices of the OAM modes in the two rings. Therefore, the tunable range of the most dispersive wavelength can be greatly enlarged by changing the doping concentration of the GeO_2 in the two rings. The highly dispersive OAM fiber can be potentially applied in plenty of fields, such as the dispersion compensation and optical buffering [41].

Methods

The HD-CRF simulations were carried out using full vector finite element method (FEM). First, the cross-section of the fiber is divided into different homogeneous subspaces, so that a simple finite element mesh is obtained after distribution. In order to describe the strength and distribution of the magnetic or electric field more precisely, as the distance of the subspace to the center is closer, their size will gradually decrease. Then use Maxwell's equation to discretize each subspace element to get a set of fundamental matrices. The combination of these fundamental matrices creates a global matrix system for the entire structure. Finally, the effective refractive index and distribution of the amplitudes and polarizations of the modes are numerically calculated, taking into account the continuity conditions at each subspace boundary.

Declarations

Data availability

All data generated or analysed during this study are included in this published article.

Author contributions statement

All the authors contributed equally in this work.

Competing interests

The authors declare no competing interests.

References

1. Yao, A. M. & Padgett, M. J. Orbital angular momentum: origins, behavior and applications. Adv. Opt. Photonics **3**, 161–204 (2011).
2. Bozinovic, N., Golowich, S., Kristensen, P. & Ramachandran, S. Control of orbital angular momentum of light with optical fibers. Opt. Lett. **37**, 2451–2453 (2012).
3. Richardson, D. J., Fini, J. M. & Nelson, L. E. Space-division multiplexing in optical fibres. Nature Photon. **7**, 354–362 (2013).
4. Li, G., Bai, N., Zhao, N. & Xia, C. Space-division multiplexing: the next frontier in optical communication. Adv. Opt. Photonics **6**, 413–487 (2014).
5. Ren, Y. *et al.* Orbital angular momentum-based space division multiplexing for high-capacity underwater optical communications. Sci. Rep. **6**, 1–10 (2016).
6. Bozinovic, N. *et al.* Terabit-scale orbital angular momentum mode division multiplexing in fibers. Science **340**, 1545–1548 (2013).
7. Willner, A. E. *et al.* Optical communications using orbital angular momentum beams. Adv. Opt. Photonics **7**, 66–106 (2015).
8. Huang, H. *et al.* Mode division multiplexing using an orbital angular momentum mode sorter and MIMO-DSP over a graded-index few-mode optical fibre. Sci. Rep. **5**, 1–7 (2015).
9. Wang, J. *et al.* Terabit free-space data transmission employing orbital angular momentum multiplexing. Nature Photon. **6**, 488–496 (2012).
10. Yue, Y. *et al.* Mode properties and propagation effects of optical orbital angular momentum (OAM) modes in a ring fiber. IEEE Photonics J. **4**, 535–543 (2012).
11. Sharma, M., Pradhan, P. & Ung, B. Endlessly mono-radial annular core photonic crystal fiber for the broadband transmission and supercontinuum generation of vortex beams. Sci. Rep. **9**, 1–12 (2019).
12. Padgett, M. & Bowman, R. Tweezers with a twist. Nature Photon. **5**, 343–348 (2011).

13. Gecevičius, M., Drevinskas, R., Beresna, M. & Kazansky, P. G. Single beam optical vortex tweezers with tunable orbital angular momentum. Appl. Phys. Lett. **104**, 231110 (2014).
14. Cvijetic, N., Milione, G., Ip, E. & Wang, T. Detecting lateral motion using light's orbital angular momentum. Sci. Rep. **5**, 1–7 (2015).
15. Xie, G. *et al.* Using a complex optical orbital-angular-momentum spectrum to measure object parameters. Opt. Lett. **42**, 4482–4485 (2017).
16. Brunet, C. *et al.* Design of a family of ring-core fibers for OAM transmission studies. Opt. Express **23**, 10553–10563 (2015).
17. Gregg, P., Kristensen, P. & Ramachandran, S. Conservation of orbital angular momentum in air-core optical fibers. Optica **2**, 267–270 (2015).
18. Guerra, G. *et al.* Analysis of modal coupling due to birefringence and ellipticity in strongly guiding ring-core OAM fibers. Opt. Express **27**, 8308–8326 (2019).
19. Ramachandran, S., Kristensen, P. & Yan, M. F. Generation and propagation of radially polarized beams in optical fibers. Opt. Lett. **34**, 2525–2527 (2009).
20. Wang, Y. *et al.* Air-Core Ring Fiber With > 1000 Radially Fundamental OAM Modes Across O, E, S, C, and L Bands. IEEE Access **8**, 68280–68287 (2020).
21. Wang, Y. *et al.* Two-Octave Supercontinuum Generation of High-Order OAM Modes in Air-Core As S Ring Fiber. *IEEE Access* **8**, 114135-114142 (2020).
22. Wang, Y. *et al.* Beyond Two-Octave Coherent OAM Supercontinuum Generation in Air-Core As_2S_3 Ring Fiber. IEEE Access **8**, 96543–96549 (2020).
23. Mashinsky, V. *et al.* Germania-glass-core silica-glass-cladding modified chemical-vapor deposition optical fibers: optical losses, photorefractivity, and Raman amplification. Opt. Lett. **29**, 2596–2598 (2004).
24. Wang, C., Wang, M. & Wu, J. Heavily germanium-doped silica fiber with a flat normal dispersion profile. IEEE Photonics J. **7**, 1–10 (2015).
25. Jain, D. *et al.* Record power, ultra-broadband supercontinuum source based on highly GeO_2 doped silica fiber. Opt. Express **24**, 26667–26677 (2016).
26. Reddy, P. H. *et al.* Fabrication of ultra-high numerical aperture GeO_2-doped fiber and its use for broadband supercontinuum generation. Appl. Opt. **56**, 9315–9324 (2017).
27. Deroh, M., Kibler, B., Maillotte, H., Sylvestre, T. & Beugnot, J.-C. Large Brillouin gain in Germania-doped core optical fibers up to a 98 mol% doping level. Opt. Lett. **43**, 4005–4008 (2018).
28. Foster, M. A. *et al.* Silicon-chip-based ultrafast optical oscilloscope. Nature **456**, 81–84 (2008).
29. Geraghty, D. F., Salem, R., Foster, M. A. & Gaeta, A. L. A simplified optical correlator and its application to packet-header recognition. IEEE Photonics Technol. Lett. **20**, 487–489 (2008).
30. Frankel, M. Y. & Esman, R. D. True time-delay fiber-optic control of an ultrawideband array transmitter/receiver with multibeam capability. IEEE Trans. Microwave Theory Tech. **43**, 2387–2394 (1995).

31. Jiang, Y. *et al.* Dispersion-enhanced photonic crystal fiber array for a true time-delay structured X-band phased array antenna. IEEE Photonics Technol. Lett. **17**, 187–189 (2004).
32. Lin, C., Kogelnik, H. & Cohen, L. G. Optical-pulse equalization of low-dispersion transmission in single-mode fibers in the 1.3–1.7-μm spectral region. Opt. Lett. **5**, 476–478 (1980).
33. Thyagarajan, K., Varshney, R., Palai, P., Ghatak, A. & Goyal, I. A novel design of a dispersion compensating fiber. IEEE Photonics Technol. Lett. **8**, 1510–1512 (1996).
34. Birks, T., Mogilevtsev, D., Knight, J. & Russell, P. S. J. Dispersion compensation using single-material fibers. IEEE Photonics Technol. Lett. **11**, 674–676 (1999).
35. Auguste, J.-L. *et al.* Conception, realization, and characterization of a very high negative chromatic dispersion fiber. Opt. Fiber Technol. **8**, 89–105 (2002).
36. Hsu, J.-M., Yao, C.-W. & Chen, J.-Z. Wavelength-tunable dispersion compensating photonic crystal fibers suitable for conventional/coarse wavelength division multiplexing systems. J. Lightwave Technol. **33**, 2240–2245 (2015).
37. Malitson, I. H. Interspecimen comparison of the refractive index of fused silica. J. Opt. Soc. Am. B **55**, 1205–1209 (1965).
38. Fleming, J. W. Dispersion in GeO_2–SiO_2 glasses. Appl. Opt. **23**, 4486–4493 (1984).
39. Afshar, S. & Monro, T. M. A full vectorial model for pulse propagation in emerging waveguides with subwavelength structures part I: Kerr nonlinearity. Opt. Express **17**, 2298–2318 (2009).
40. Zhang, L., Yue, Y., Xiao-Li, Y., Beausoleil, R. G. & Willner, A. E. Highly dispersive slot waveguides. Opt. Express **17**, 7095–7101 (2009).
41. Baba, T. Slow light in photonic crystals. Nature Photon. **2**, 465–473 (2008).

Figures

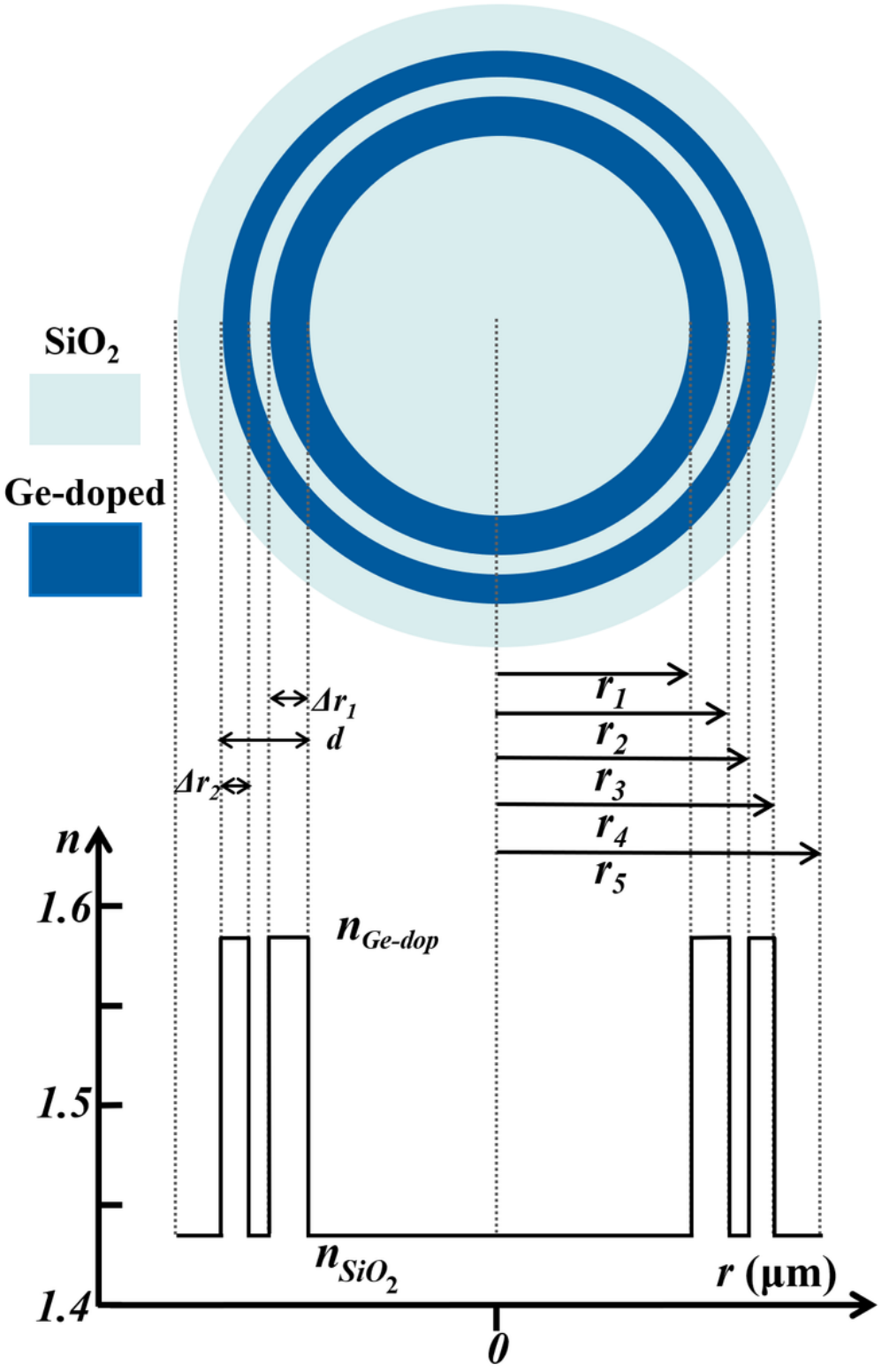

Figure 1

Transverse section and material refractive index distribution of the designed germanium-doped OAM HD-CRF.

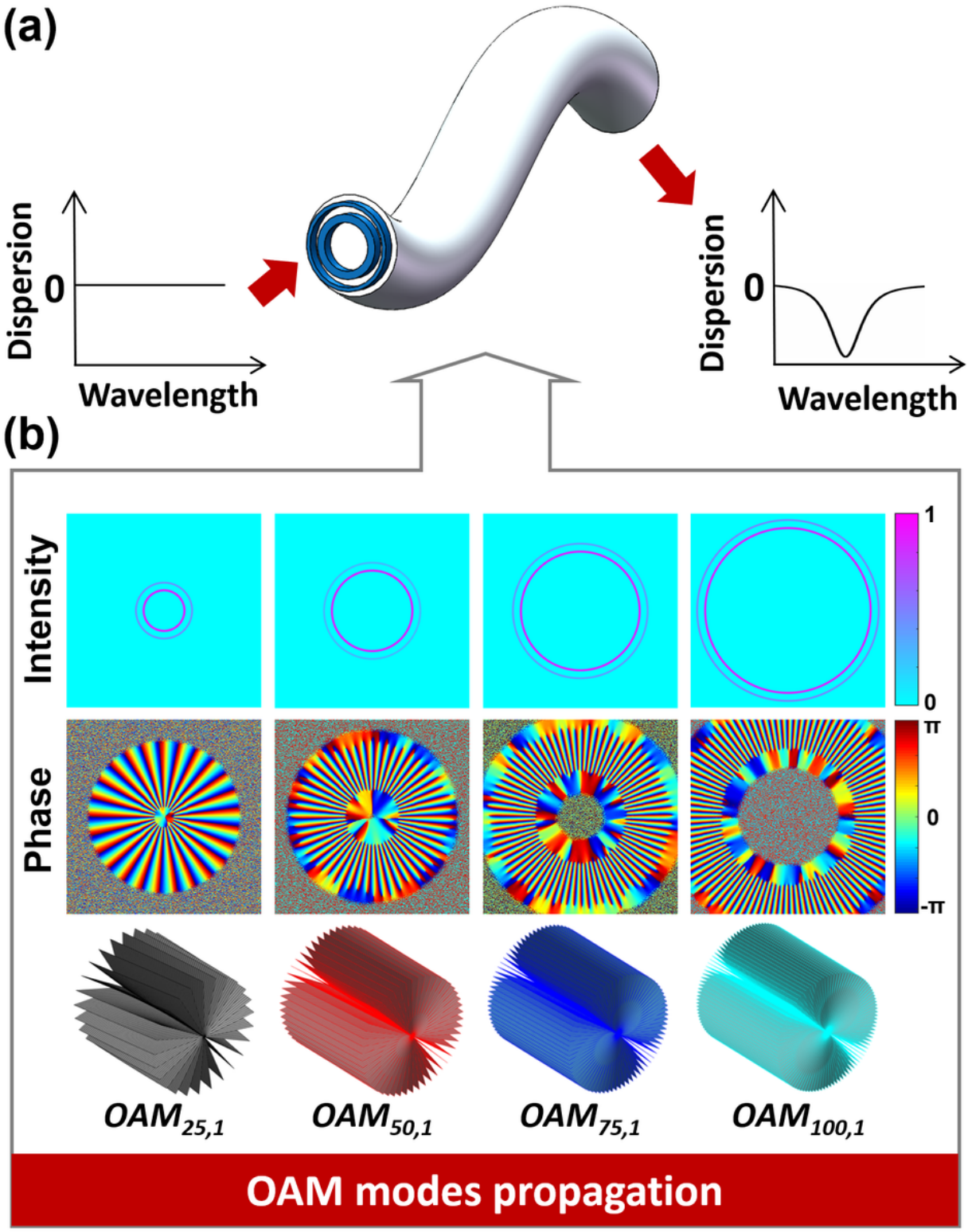

Figure 2

(a) Concept of the designed HD-CRF for propagating OAM modes with negative dispersion; (b) Mode field distributions of different OAM modes in the optimized fibers with their corresponding geometric variables at λ_0.

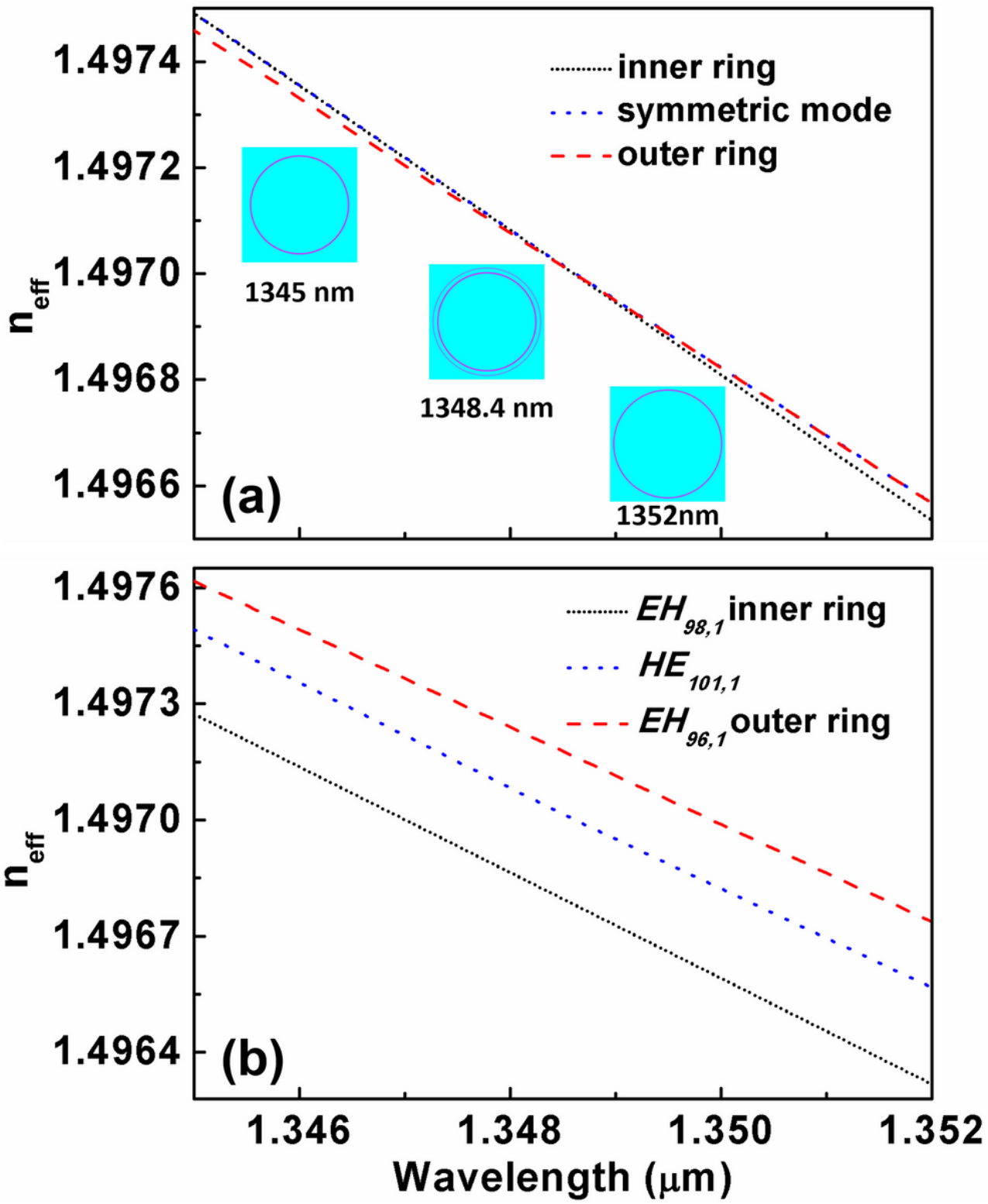

Figure 3

(a) $OAM_{100,1}$ mode Effective refractive indices and intensity distributions of proposed fiber versus wavelength; (b) Effective refractive indices of eigenmodes supported by the designed fiber.

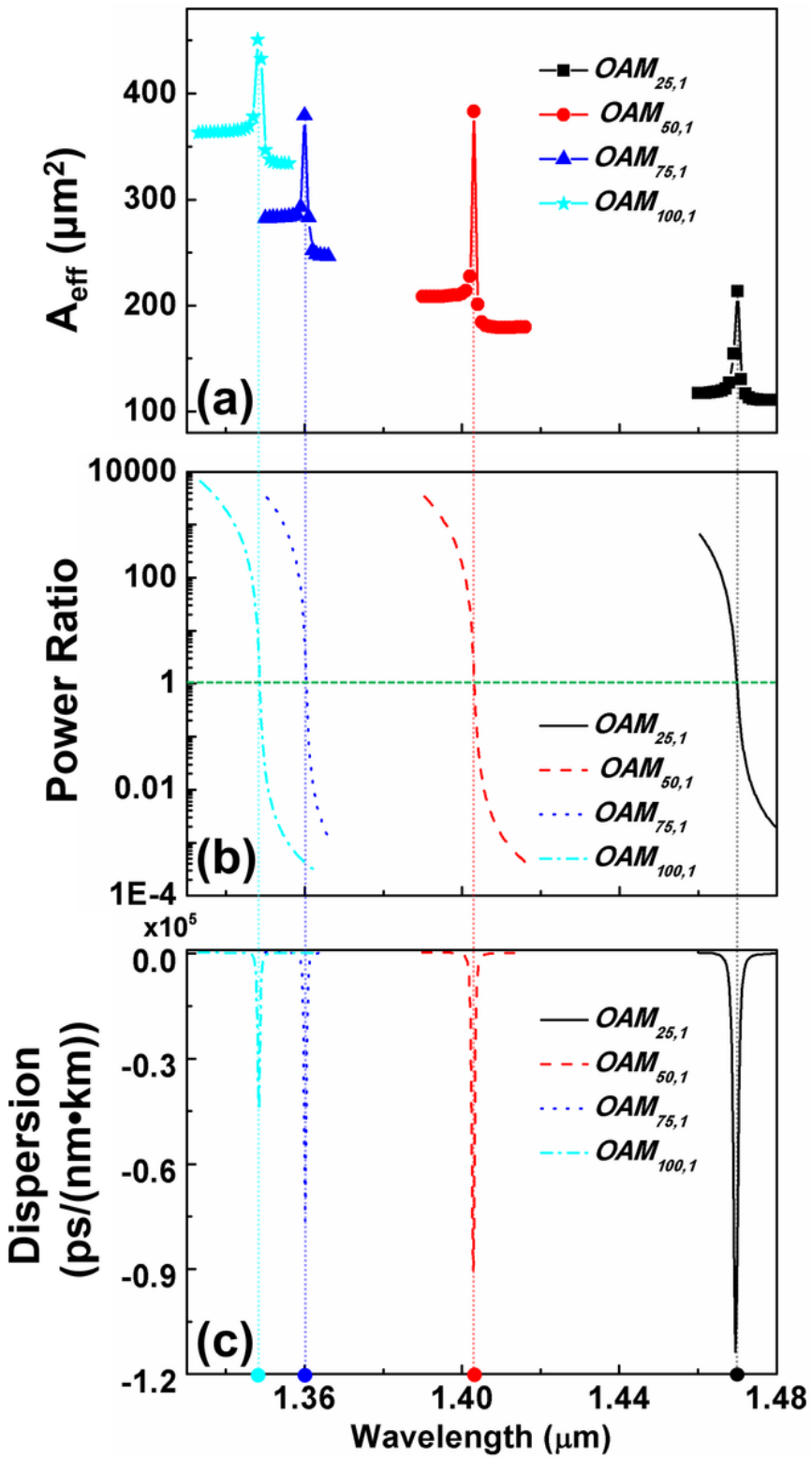

Figure 4

(a) Effective mode area, (b) ratio of power integral in the high-index ring near the core to that in ring near the fiber cladding, and (c) chromatic dispersion of the OAM modes with different *l* in the proposed fibers with their corresponding adjusted geometric variables.

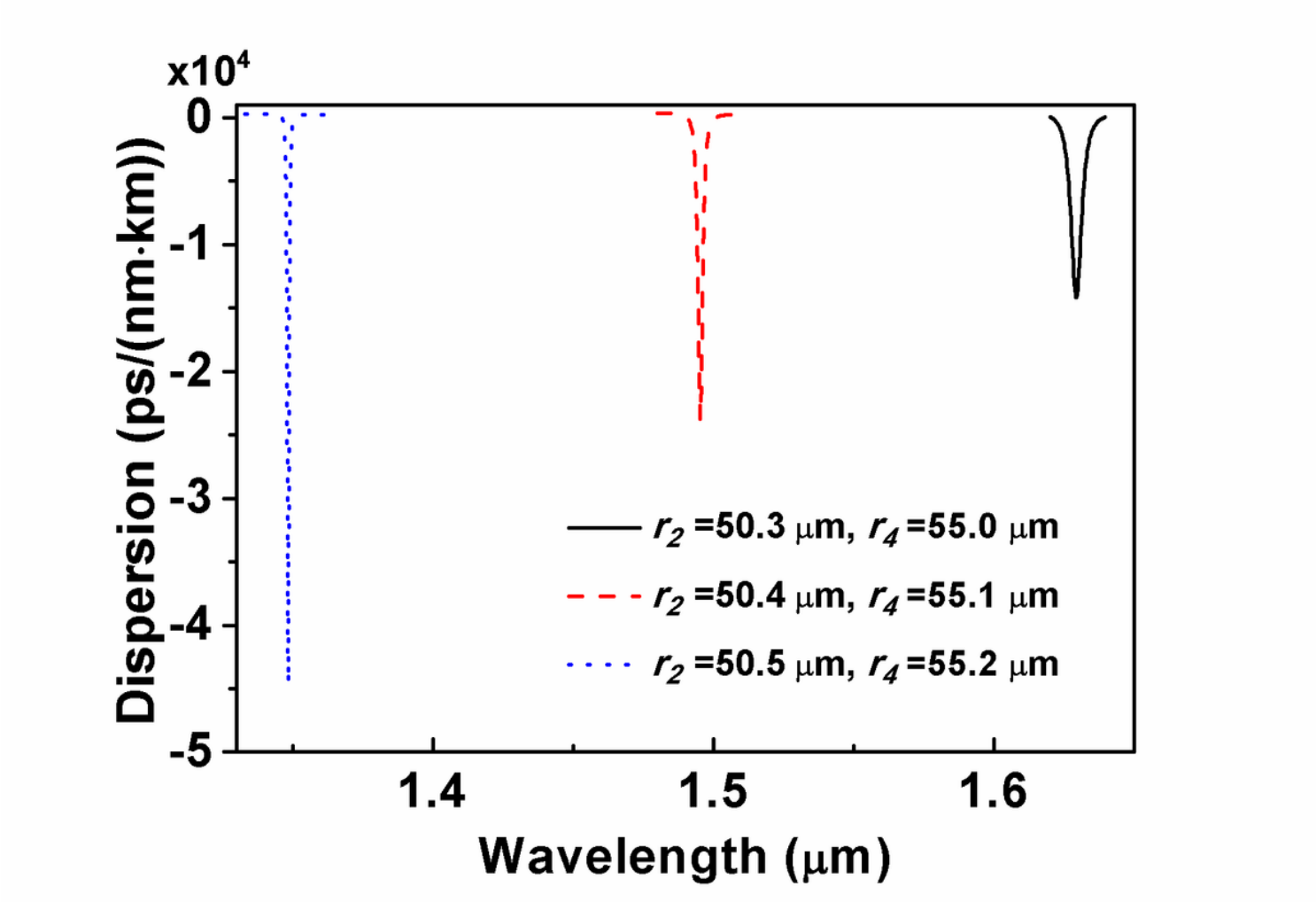

Figure 5

Dispersion profiles of $OAM_{100,1}$ mode versus wavelength for different values of Δr_1 and Δr_2 with r_1 = 49 μm, r_3 = 54 μm.

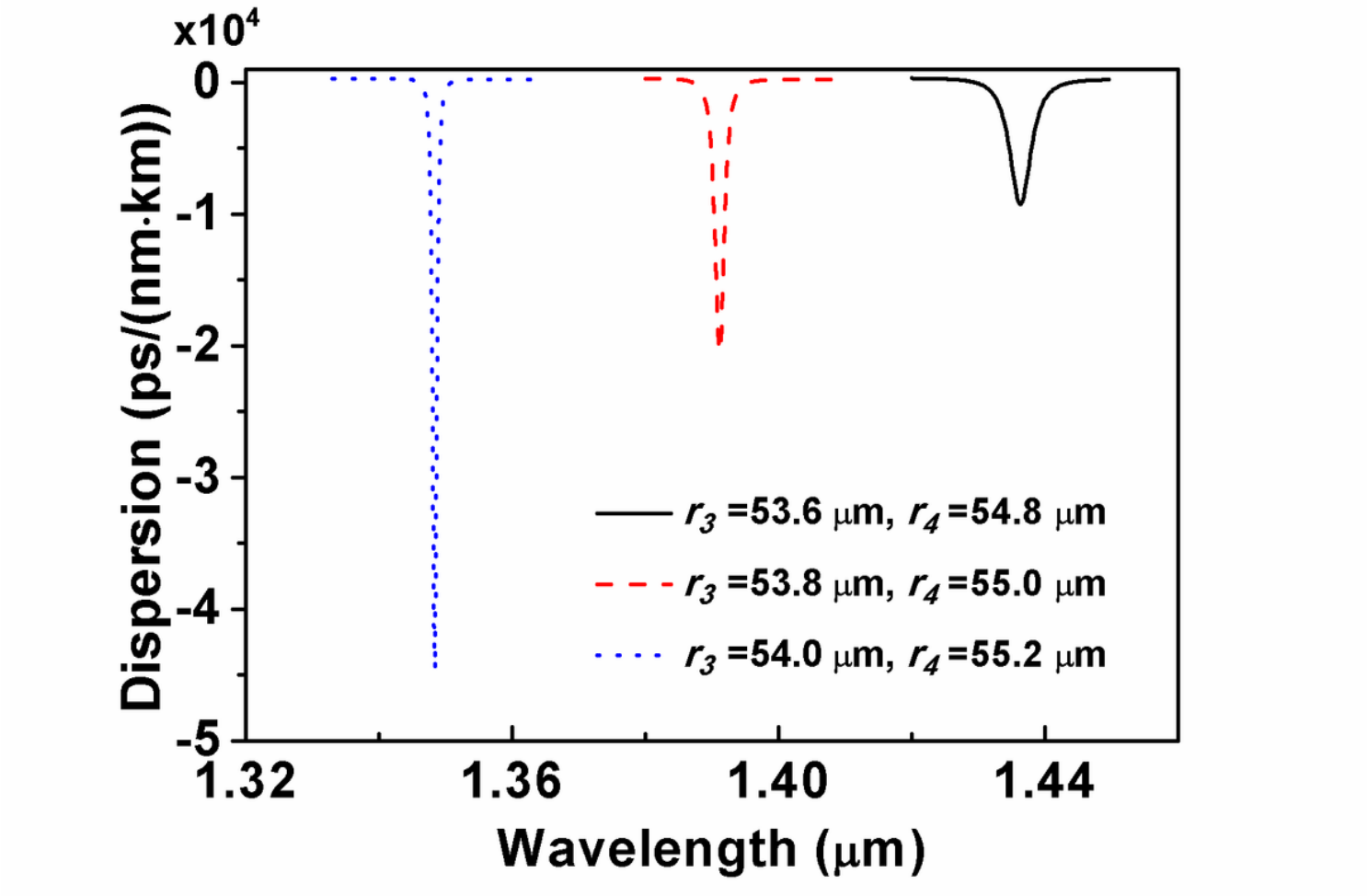

Figure 6

Dispersion profiles of $OAM_{100,1}$ mode versus wavelength for different values of r_3 with r_1 = 49 μm, r_2 = 50.5 μm and Δr_2 = 1.2 μm.

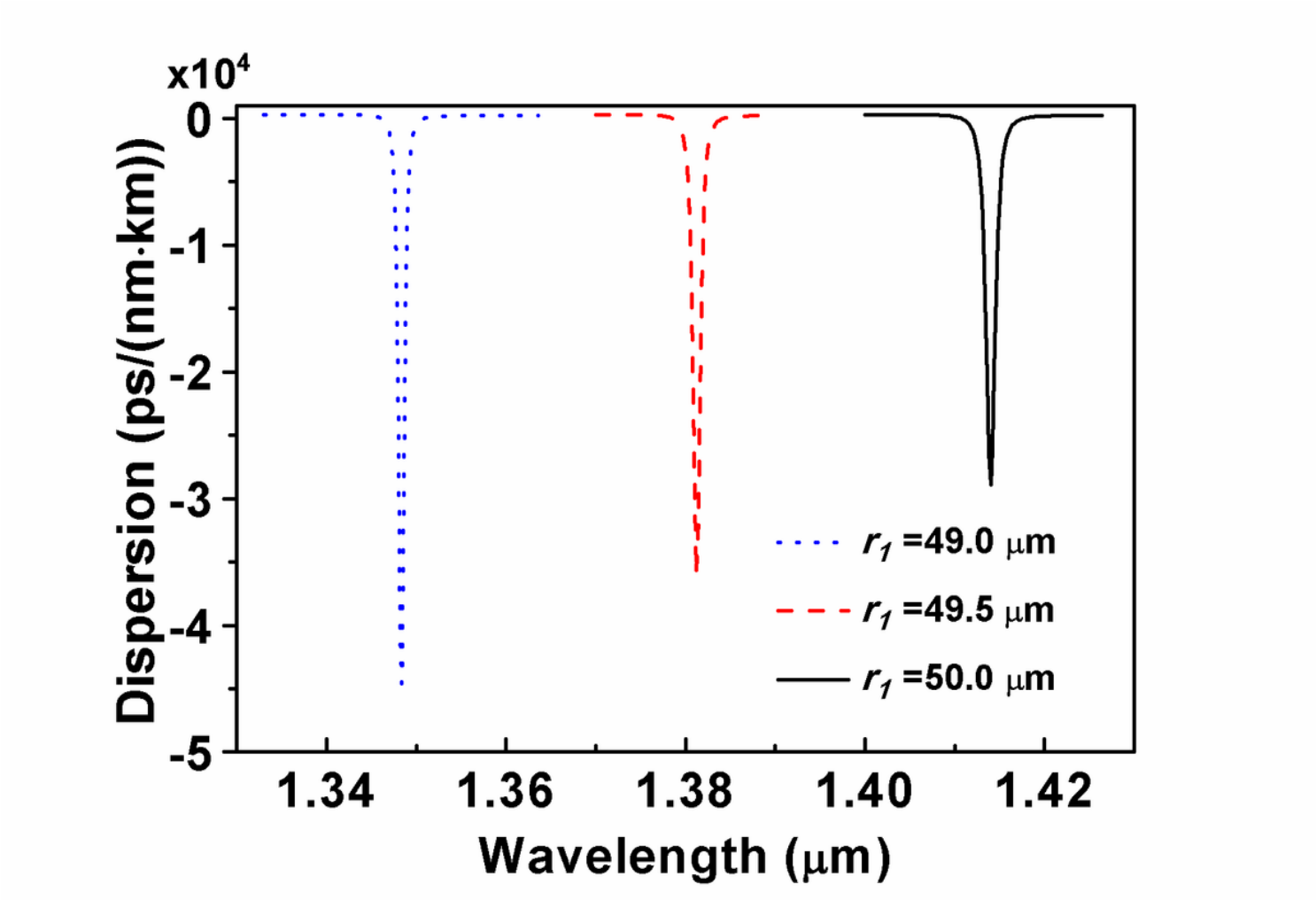

Figure 7

Dispersion profiles of $OAM_{100,1}$ mode versus wavelength for different values of r_1 with Δr_1 = 1.5 μm, Δr_2 = 1.2 μm, d = 5 μm.

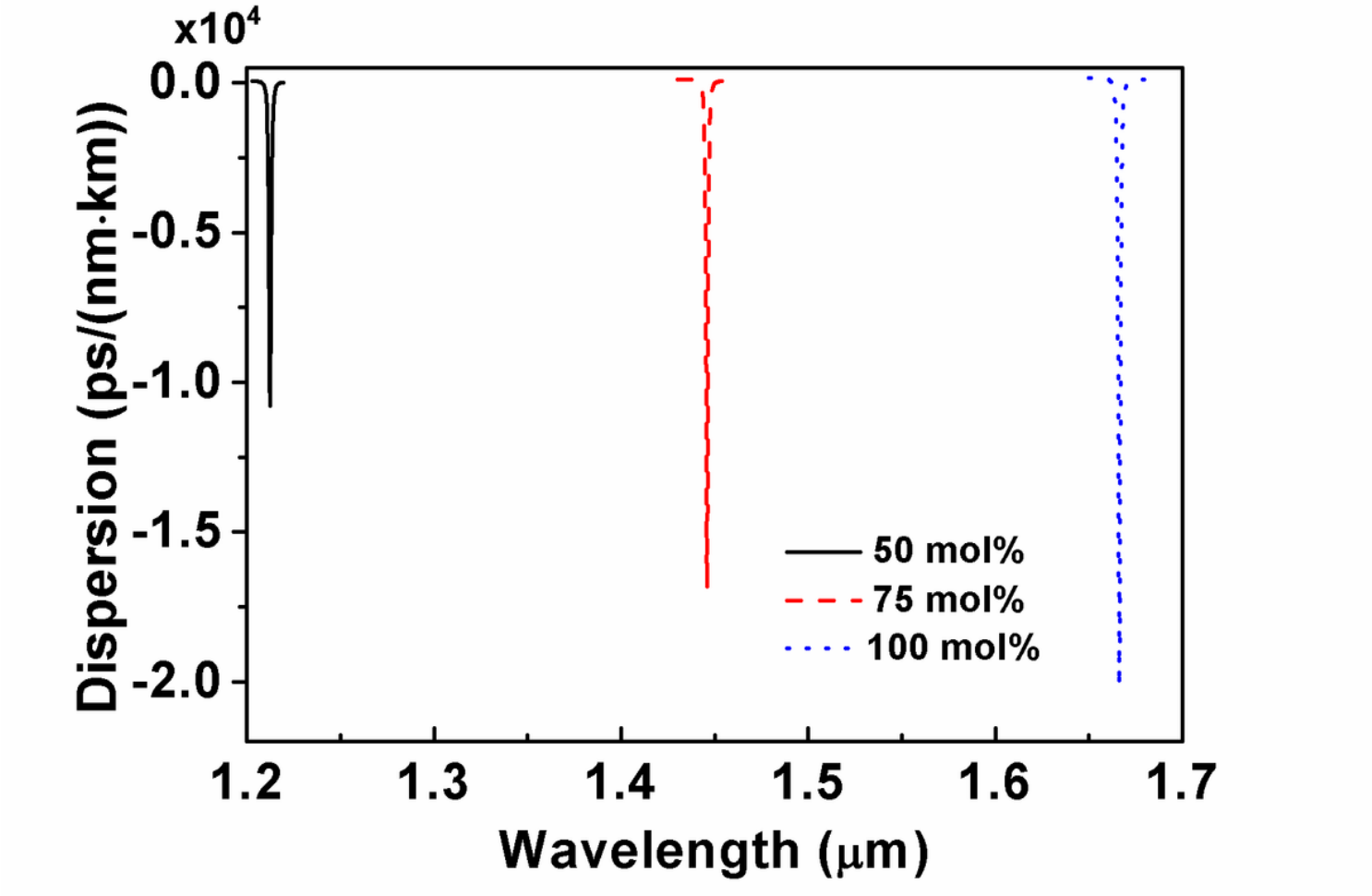

Figure 8

Dispersion profiles of $OAM_{65,1}$ mode versus wavelength for different values of GeO_2 mole fractions with r_1 = 50 μm, r_2 = 51.5 μm, r_3 = 56 μm and r_4 = 57.3 μm.